Photodissociation of Conformer-Selected Ubiquitin Ions Reveals Site-Specific *Cis/Trans* Isomerization of Proline Peptide Bonds

Stephan Warnke,[†] Carsten Baldauf,[†] Michael T. Bowers,[‡] Kevin Pagel,*[,†,#] and Gert von Helden*[,†]

[†]Fritz-Haber-Institut der Max-Planck-Gesellschaft, Faradayweg 4-6, 14195 Berlin, Germany

[‡]Department of Chemistry and Biochemistry, University of California, Santa Barbara, Santa Barbara, California 93106, United States

Ⓢ *Supporting Information*

ABSTRACT: Ultraviolet photodissociation (UVPD) of gas-phase proteins has attracted increased attention in recent years. This growing interest is largely based on the fact that, in contrast to slow heating techniques such as collision induced dissociation (CID), the cleavage propensity after absorption of UV light is distributed over the entire protein sequence, which can lead to a very high sequence coverage as required in typical top-down proteomics applications. However, in the gas phase, proteins can adopt a multitude of distinct and sometimes coexisting conformations, and it is not clear how this three-dimensional structure affects the UVPD fragmentation behavior. Using ion mobility−UVPD−mass spectrometry in conjunction with molecular dynamics simulations, we provide the first experimental evidence that UVPD is sensitive to the higher order structure of gas-phase proteins. Distinct UVPD spectra were obtained for different extended conformations of 11[+] ubiquitin ions. Assignment of the fragments showed that the majority of differences arise from *cis/trans* isomerization of one particular proline peptide bond. Seen from a broader perspective, these data highlight the potential of UVPD to be used for the structural analysis of proteins in the gas phase.
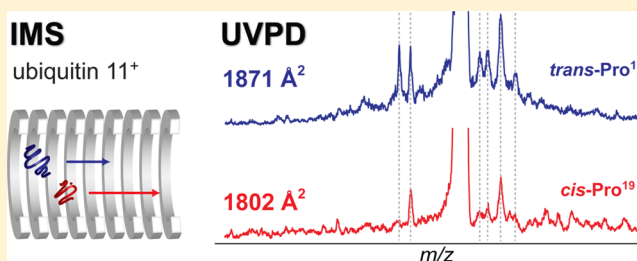
■ INTRODUCTION

Understanding the structure and dynamics of proteins is one of the greatest challenges in the life sciences. To experimentally tackle this, a large variety of techniques to investigate samples in the condensed phase have been developed. In the last decades, techniques to study proteins in the absence of solvent, that is, in the gas phase, have emerged as promising additions that provide complementary information. Most of these methods rely on gentle ionization techniques such as electrospray ionization (ESI) followed by mass spectrometry (MS), and together with methods to isolate, energize, and fragment gas-phase molecules, MS is today the work-horse technique in "omics" research.[1,2]

MS by itself provides only indirect information about higher order structure such as the hydrogen bonding network and the folding of the molecule. To investigate such structural aspects, MS can be combined with optical spectroscopy or ion mobility spectrometry (IMS) methods. When infrared spectroscopy is used, for example, details about the secondary structure can be obtained.[3] IMS methods on the other hand can yield complementary information on the overall shape of the molecule in the form of the absolute collision cross section (CCS).[4−6] Further, IMS allows one to separate species of the same mass-to-charge (*m/z*) ratio that exhibit multiple conformations.

Performing experiments in the gas phase offers several distinct advantages compared with condensed-phase studies. When mass spectrometry is employed, molecules with a specific *m/z* can be selected. With IMS methods on the other hand, molecules with specific CCSs can be isolated. Combining the two methods allows for the selection of biomolecular ions with defined protonation and aggregation states, as well as selected molecular shapes.[7] Such selectivity is often difficult to achieve in the condensed phase, where different protonation states, conformations, and aggregation states can be in a dynamic equilibrium for which typically only a distribution can be probed.

There are, however, also distinct disadvantages that are encountered in gas-phase studies. First of all, due to inherent low sample densities, nuclear magnetic resonance (NMR) type experiments can presently not be performed on samples of gas-phase biological molecules. X-ray diffraction experiments are promising but still far from being mature since very specialized X-ray sources will be required.[8] Most importantly, however, when one tries to elucidate higher order structures, it has to be kept in mind that the structural preferences of biological molecules in the gas phase may be different from those in the condensed phase, because the global free energy minimum in solution is usually only a local minimum in the absence of solvent.[9,10] Nonetheless, it has been shown in many experiments that when the molecules are handled gently, condensed-phase structural elements can be retained after transfer into the gas phase.[10−12]

In the recent past, ultraviolet photodissociation (UVPD) in conjunction with tandem MS (MS/MS) emerged as a promising tool to analyze the primary structure of proteins.[13] In contrast to widely used low-energy dissociation techniques such as collision induced dissociation (CID), the cleavage propensity after absorption of UV light is distributed over the entire protein sequence, which can lead to a very high sequence coverage and thus might allow for top-down protein sequencing.[14−17] Furthermore, UVPD can be applied to a large variety of instruments with only relatively few modifications. It is, however, not known whether the UVPD fragmentation behavior is influenced by the higher order structure of the molecule. If so, can UVPD data be used to deduce direct structural information? For a multitude of reasons, this question is difficult to address. The observed fragmentation pattern as well as the conformation of the molecule will both depend on the charge state. As a result, it is very difficult to disentangle the influence of the charge and the conformation on the fragmentation behavior within one experiment.

Here, we present the first UVPD fragmentation spectra of protein ions, which are both m/z and conformer selected. Using the well-characterized 76-residue protein ubiquitin, we show that the gas-phase structure of the protein has a considerable impact on the fragments formed via UVPD, with the most significant differences arising from cleavage around one particular proline residue.

■ MATERIALS AND METHODS

Samples. Human ubiquitin was purchased from R&D Systems and used without further purification. Solvents were purchased from Sigma-Aldrich. For electrospray ionization, an aqueous 1 mM ubiquitin stock solution was diluted with water/methanol, v/v 50/50, to yield a concentration of 10 μM. Formic acid (1.5%) was added to generate high charge states.

Ion Mobility−Mass Spectrometry (IM-MS). A drift-tube instrument similar to the one used here has been described previously.[18] Ions are generated in a nanoelectrospray ionization source (nESI) and transferred into the vacuum. An electrodynamic ion funnel collects and pulses ions into the drift region where they drift through helium buffer gas under the influence of a weak electric field. A second electrodynamic ion funnel guides the conformer-separated ions into ultrahigh vacuum. Here, ions of specific drift times can be selected following m/z selection by a quadrupole mass spectrometer. UVPD via irradiation with a 193 nm excimer laser pulse occurs approximately 100 μs prior to ToF mass analysis. The UV pulse length and energy are about 5 ns and 1 mJ, respectively, and the beam diameter is about 1 cm. Under those conditions, the absorption of multiple photons is not expected. Further, the laser power dependence of the fragmentation yield is observed to be linear, in line with a one-photon process. A detailed description of the experiment can be found in the Supporting Information.

Molecular Dynamics (MD) Simulations. All MD simulations and part of the analysis were carried out with the Gromacs suite of programs (version 4.6.3).[19] The ff99SB-ILDN[20] parameter set of the Amber force field was used for the protein. The four-ubiquitin models described here were briefly equilibrated, and then for each of the four systems (ttt, ctt, tct, ttc), six MD simulations of 100 ns were performed with an integration step size of 0.5 fs. The temperature was 300 K, coupled to the velocity-rescaling thermostat by Bussi, Donadio, and Parrinello.[21] No cut-offs for nonbonded interactions and no bond constraints were applied. Only the last 60 ns of the 100 ns trajectories were considered for analysis.

■ RESULTS AND DISCUSSION

Ubiquitin in the Gas Phase. Ubiquitin is, as its name suggests, one of the most commonly occurring proteins in eukaryotes and has as such been studied extensively in the gas phase using a variety of techniques.[17,22−25] Pioneering work in the groups of Clemmer and Bowers for example showed that ubiquitin can adopt a multitude of defined and partially interchangeable conformations in the gas phase[10,24,26−28] of which some are closely linked to those of ubiquitin in the condensed phase.[24,29] A particularly interesting example of those gas-phase conformers is a group of structures occurring for high charge states. There, structures are observed that, unlike ubiquitin in its native fold, are not compact but rather extended.[24,28] In the condensed phase an extended structure with a native-like β-hairpin motif near the N-terminus and a predominantly helical C-terminal domain can be observed in water/methanol mixtures.[30−32] The structure of this so-called A-state is compatible with the sizes of some of the highly charged ubiquitin ions in the gas phase as determined in IM-MS experiments.[24] Here, we investigate ubiquitin in the 11$^+$ charge state for which two dominant gas-phase conformers with structures compatible with the A-state have been observed previously.[24]

Photodissociation of Conformer-Selected Ubiquitin. Ubiquitin ions are brought into the gas phase via nano-electrospray ionization (nESI) and transferred into the low-pressure environment of the experimental apparatus. Here, the ions are trapped and short pulses are released into a drift region, which they traverse at drift velocities that are related to their corresponding size. Subsequently, the ions exiting the drift region are transferred to high vacuum where m/z selection by a quadrupole mass filter takes place. After mass selection, the ions are either directly transferred to a detector or irradiated by a UV excimer laser at 193 nm followed by time-of-flight mass analysis of the resulting fragments.

In Figure 1, an arrival time distribution (ATD) of ubiquitin ions in the 11$^+$ charge state is shown. Clearly, two peaks can be
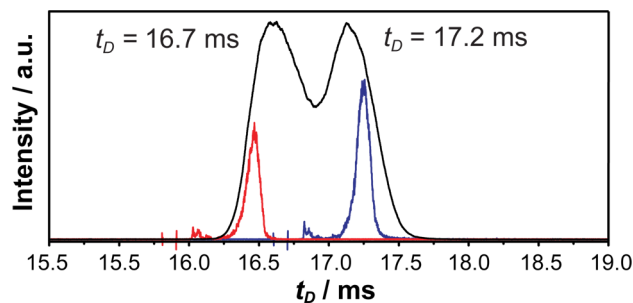

Figure 1. Arrival time distribution (ATD) of 11$^+$ ubiquitin. For conformer-selective photodissociation experiments, 100 μs fractions of each species were isolated (red and blue).

seen, resulting from two distinct conformations or conformational families. Their corresponding drift times can be converted into CCSs, which both are comparable to those determined previously for extended structures of ubiquitin.[24,26]

From the two peaks in the ATD shown in Figure 1, a small 100 μs fraction can be isolated by electric deflection of the other ions. The isolated fraction representing the conformer occurring at earlier times (16.7 ms) and the isolated fraction representing the more extended conformer (17.2 ms) are shown as red and blue traces in Figure 1, respectively. Those
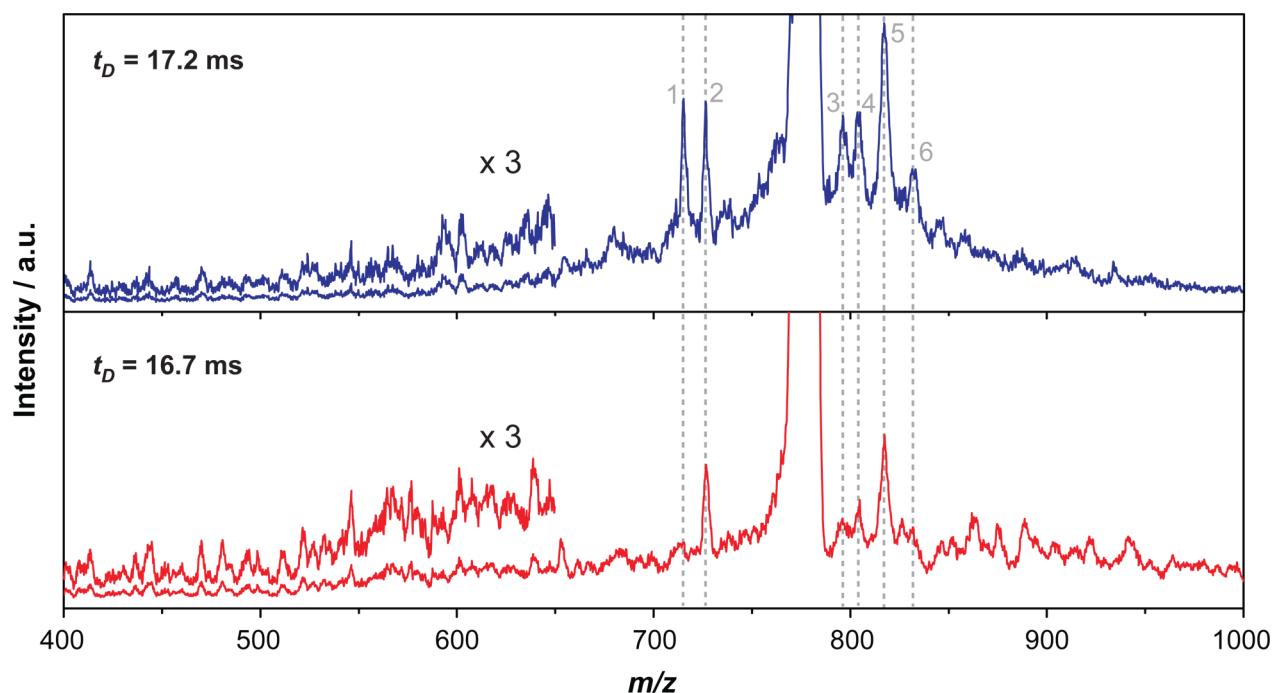
Figure 2. UVPD spectra of conformer selected 11^+ ubiquitin. Spectra are shown for the compact conformation (t_D = 16.7 ms, lower panel, red) and for the more extended conformation (t_D = 17.2 ms, upper panel, blue). The dashed lines indicate the positions of the most prominent differences at m/z 716 (#1), 726 (#2), 795 (#3), 805 (#4), 817 (#5), and 833 (#6).
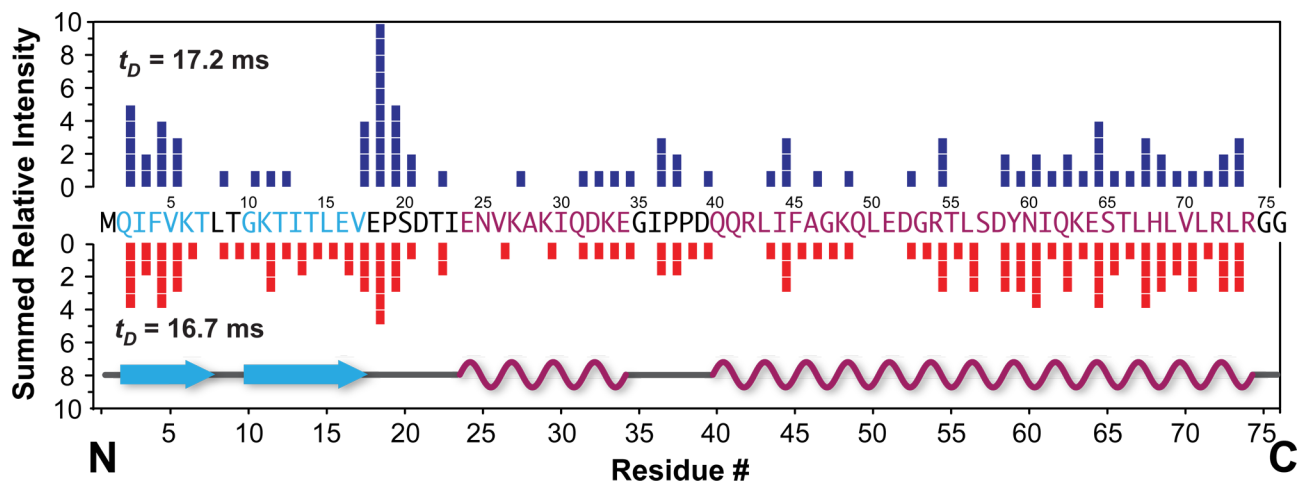

Figure 3. UVPD fragmentation propensity of the two conformers of 11^+ ubiquitin. The bars show the combined relative intensities of all fragments that originate from the same cleavage site for the compact conformer (t_D = 16.7 ms, lower panel, red) and the more extended form (t_D = 17.2 ms, upper panel, blue). The structure shown in the lower part of the figure is based on the A-state.

m/z and conformer selected ions can now be irradiated with a single 193 nm pulse of an ArF excimer laser, and the resulting photofragmentation spectra are shown in Figure 2. Both spectra consist of many peaks, some of which are only partially resolved. Some peaks clearly occur in both spectra; others, however, are prominent in only one. Among the most prominent features and striking differences are the peaks at m/z 716, 726, 795, 805, 817, and 833, which are numbered consecutively from 1 to 6 in Figure 2.

The observation of a different fragmentation behavior is interesting by itself — especially when considering that conformer-selective CID does not yield distinct fragmentation patterns[33] (see also Figure S5, Supporting Information). The mass spectra in Figure 2 both stem from the same molecules in

the same charge state that merely differ in conformation. Those two conformers might also differ in their internal charge distribution. Both factors could influence the observed fragmentation pattern and are typically difficult to disentangle. The impact of distinct charge localization has recently been investigated extensively for a small model peptide system.[34] In that study, structural differences could not be linked to different charge distributions. Further, the approach applied there is difficult to transfer to the here considered larger species. Here, our goal is to determine whether structural differences are sufficient to explain the differences observed in the UV induced fragmentation patterns of the two distinct ATD peaks.

Fragment Assignment. To classify the differences in the mass spectra according to the underlying cleavage position, it is

necessary to assign the corresponding fragments. Due to the limited resolution of the spectra, an assignment purely based on the data presented here is difficult. With the aid of high-resolution UVPD spectra of non-conformer selected ions obtained by the group of Jennifer S. Brodbelt,[14] however, we are able to unambiguously identify all prominent and most of the weaker features (for a list of all assigned fragments see Table S1, Supporting Information). Fragment #3 in Figure 2, for example, is an N-terminal a_{36} fragment (5+) occurring from the cleavage of the peptidic backbone between residues Ile[36] and Pro[37]. The most apparent differences in the fragment spectra, however, originate from cleavage around a single residue: Pro[19]. The corresponding fragments are y_{57} (#1, 9+, and #4, 8+), y_{58} (#2, 9+, and #5, 8+), and y_{59} (#6, 8+), which are formed via cleavage of the peptide bonds between the residues Pro[19]–Ser[20], Glu[18]–Pro[19], and Val[17]–Glu[18] respectively. Based on this assignment, it can, therefore, be concluded that differences in the fragmentation behavior around Pro[19] are responsible for the majority of differences in the mass spectra in Figure 2.

In order to provide a semiquantitative picture about the prevalence of cleavages along the sequence, we assigned a relative intensity to each identifiable and assignable peak in the mass spectra using values from 0 to 3. In this scheme, 0 means no distinct peak and 1 a clearly visible peak. The six intense fragment peaks in Figure 2 were assigned a relative intensity of 2 and, if differentiation between fragment abundances was necessary, the highest intensity level 3 was assigned (relative intensities are included in the list of assigned fragments in Table S1, Supporting Information). Subsequently, the intensities were grouped according to the cleavage position along the sequence, and the corresponding histogram plot is shown in Figure 3.

One clear result is that sequence coverage is generally very high. This is in good agreement with previous studies, which showed that for ubiquitin, a coverage of almost 100% can be achieved.[14] Both conformers also feature an enhanced formation of C-terminal fragments as well as a lower cleavage propensity for the middle part of the protein. However, there are also very clear differences, which on the basis of our crude intensity assignment can be considered relevant when the relative intensity varies by more than two. The most prominent of these differences is the enhanced cleavage around Pro[19] for the higher CCS conformer as already apparent in Figure 2. This difference is especially pronounced at the N-terminal side between Glu[18] and Pro[19] with a summed relative intensity of 5 for the lower and 10 for the higher CCS conformer. Interestingly, it has been observed previously that Xxx–Pro peptide bonds can show an enhanced cleavage propensity upon activation using slow heating techniques such as CID.[35] Even though this proline effect has been shown to not be relevant in UVPD,[16] we here observe a strong preference for cleavage of the Glu[18]–Pro[19] bond, while no such preference is observed for the Xxx–Pro bonds of Pro[37] and Pro[38].

The Special Role of Pro[19]. Proline generally plays a very special role in protein folding. In peptides, its heterocyclic backbone considerably restricts the conformational flexibility, which is the reason for proline to be often involved in the formation of loops and turns. In addition, while all other amino acids almost exclusively form *trans* peptide bonds, a considerable amount of Xxx–Pro peptide bonds are found to exist in *cis* conformation (10–40%). For ubiquitin in the condensed phase, *cis/trans* isomerization of peptide bonds

preceding proline has been found to play an important role in the folding dynamics.[36−38] For unfolded, condensed-phase ubiquitin, about 9% of Pro[19], 14% of Pro[37], and 19% of Pro[38] are involved in *cis* peptide bonds.[37] Pro[19], however, occupies a somewhat strategic position for folding since the native hydrogen bonded structure can only be formed when Pro[19] is preceded by a *cis* peptide bond.[37] In contrast, *cis* peptide bonds preceding Pro[37] and Pro[38] are less important for the overall structure.[37] Furthermore, *cis/trans* isomerization is responsible for rather slow folding dynamics and represents a kinetic bottleneck.[37]

Also in the gas phase, *cis/trans* isomerization of the Xxx–Pro peptide bond was recently shown to significantly influence the structure of smaller peptides. A detailed analysis of different variants of the nonapeptide bradykinin, for example, revealed that *cis/trans* isomerization of prolyl–peptide bonds is responsible for the formation of multiple distinct coexisting gas-phase conformations.[34] Analysis of a wide number of proline-containing peptides furthermore showed that this effect is rather general and not limited to bradykinin.[39] Furthermore, we have recently demonstrated how *cis/trans* isomerization is influenced by interactions with monovalent cations.[40]

The observation of two (or more) peaks in an ATD means that two (or more) different conformations with different cross sections are stable in the gas phase and do not interconvert on a millisecond time scale at 300 K. This implies that rather large free energy barriers separate their corresponding conformational space. A large number of hydrogen bonds that need to be broken simultaneously in order to change conformation could give rise to such a barrier. When the structural differences are large, as for example for a folded and extended structure, this would be expected. In the case of ubiquitin 11+, however, both structures are extended, for which case it is much more difficult to imagine a substantial free energy barrier that is governed by differences in the hydrogen bond pattern. The observation that both structures generating the ATD in Figure 1 mostly show differences in the UVPD fragmentation behavior around Pro[19] points to a special role of this residue. *Cis/trans* isomerization of an associated peptide bond could explain both the apparent presence of a large free energy barrier and the difference in fragmentation behavior of the two conformers.

MD Simulations. In order to shed more light on the possible role of proline *cis/trans* isomerization, we performed molecular dynamics (MD) simulations of ubiquitin with the peptide bond preceding residues Pro[19], Pro[37], and Pro[38] in all *trans-* (*ttt*) as well as mixed *cis/trans* (*ctt*, *tct*, and *ttc*) conformations using the Amber force field (ff99SB-ILDN)[20] and the program package Gromacs.[19] For most charge states of ubiquitin, many possibilities of how protons are distributed over the various basic sites exist. The 11+ charge state is an exception, however, since 11+ is very likely formed by protonation of all four arginines, all seven lysines, and the N-terminus, with the C-terminus being the only deprotonated site. As starting point, structures resembling those of the condensed phase A-state were chosen as described before.[41−43] For each *ttt*, *ctt*, *tct*, and *ttc* conformer, six MD runs at a temperature of 300 K with a duration of 100 ns were performed. Generally, in all simulations, structures remained in conformations that featured the secondary structure of the A-state, namely, an N-terminal β-hairpin that ranges almost to Pro[19] and two helical segments that are extended by charge repulsion of the protonated side chains of the lysine and arginine residues. The simulations of the individual *cis/trans* conformer types

reveal local structural differences around the proline residues. *Cis/trans* isomerization of the peptide bonds around proline is not observed to occur over the course of a simulation.

For quantitative comparison with the experimental data, theoretical CCSs of the four conformers *ttt, ctt, tct,* and *ttc* were obtained by averaging CCS values of 3600 structures taken at 0.1 ns intervals from the MD trajectories (the first 40 ns of the trajectory were left for equilibration and were not considered in the analysis).

Figure 4 shows the ATD of 11^+ ubiquitin where the time axis is converted into CCS; the vertical lines represent the
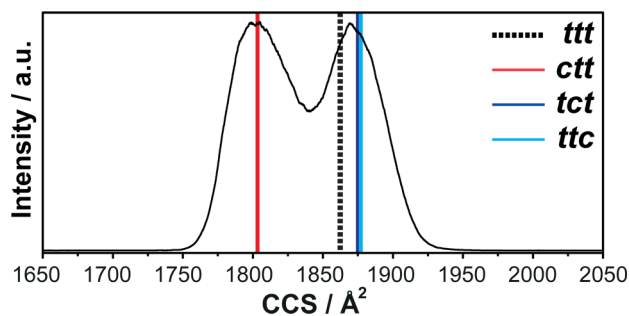

Figure 4. CCSs of 11^+ ubiquitin. The time axis in the ATD was converted to CCS, and calculated CCSs of four types of structures are shown as lines. For details, see text.

calculated CCSs of the *ttt*, as well as the *cis* Xxx−Pro bond containing structures *ctt, tct,* and *ttc*. CCS calculations were performed using the exact hard sphere scattering (EHSS) model,[44] and the resulting cross sections were scaled by 0.97. Surprisingly, only the structure with a *ctt* conformation yields a CCS that is substantially different from the all-*trans* (*ttt*) species. Considering the estimated relative error of the method of about 1%, the CCSs of the *tct* and *ttc* conformers are virtually indistinguishable from those of the all *trans* species *ttt*. The absolute values of the calculated CCSs might suffer from systematic errors in the EHSS model as well as in the geometries obtained from the MD simulations. The relative differences between the *ctt* and the other conformations should, however, suffer much less from those systematic errors. Thus, it is likely that the more compact conformer (the left fraction of the ATD) corresponds to the conformer of ubiquitin 11^+ with the peptide bond preceding Pro[19] in *cis* conformation, while the more extended conformer (the right fraction) is due to molecules with the peptide bond preceding Pro[19] in *trans* conformation.

Implications for the Fragmentation Mechanism. How can the conformational change in Pro[19] peptide bonds from *trans* to *cis* give rise to such significant changes in the UVPD signature? One possibility is that the UV absorption behavior of the molecule changes with *cis/trans* isomerization at Pro[19]. A shift in band position, a difference in oscillator strength, or a different nature of the excited state between the *cis* and *trans* peptide bond could result in differing fragmentation propensities.

A second reason for a difference in fragmentation behavior around the Pro[19] residue could be the UVPD mechanism itself. After photoexcitation, an excited electronic state will either induce direct dissociation or undergo a transition to the ground electronic state, followed by an intramolecular vibrational redistribution (IVR) of the energy gained from photon absorption (6.4 eV). This amount of energy when distributed

over all vibrational modes of the molecule in its electronic ground state is probably not enough to cause dissociation on our experimental time scale. Further, the barrier for *cis/trans* isomerization is typically 50−80 kJ mol^{-1},[45] several times lower than that required for dissociation. Thus, if dissociation occurs from the electronic ground state, it would occur from a hot molecule that likely had the opportunity to undergo *cis/trans* isomerization. In that case, one would expect a similar fragmentation behavior for originally *cis* or *trans* molecules. However, a difference in the branching ratio between dissociation from an excited electronic state and transition back to the ground state could result in a different fragmentation behavior. In that case, an electronic excitation around the *cis* peptide bond would have a higher propensity for relaxation and therefore show less fragmentation.

A third possible explanation arises from differences in the local structure of the molecules. Representative structures of the *ctt* and *ttt* molecules are shown in Figure 5A. In the *ctt* conformation, a stable turn-like structure around Pro[19] is formed, which is conserved over the entire duration of the simulation. This turn promotes multiple hydrogen bond formation in the N-terminal region of the protein. On the other hand, when the peptide bond preceding Pro[19] is in *trans* conformation, no hydrogen-bonding networks in the proximity of the Pro[19] residues are found. In Figure 5B upper panel, the number of contacts (all atoms closer than 0.3 nm) between two fragments after hypothetical cleavage of a peptide bond is plotted as a function of the cleavage position. For all structures, this plot shows a maximum in the number of contacts for a cleavage near the turn of the β-sheet segment, as the two adjacent strands are closely linked with each other. All along the backbone, the *ttt, tct,* and *ttc* conformations have a very similar number of contacts between their hypothetical N- and C-terminal fragments, in line with their very similar structures and CCSs. The *ctt* molecule on the other hand shows an enhanced number of contacts up to the end of the β-sheet region, most pronounced around the Pro[19] residue. In Figure 5B, lower panel, the difference in the number of contacts between *ttt* and the other structures is shown. Clearly, a large enhancement for *ctt* around Pro[19] is observed. That is, the N- and C-terminal fragments formed via cleavage around Pro[19] are located in close spatial proximity with an enhanced number of noncovalent contacts. Enhanced hydrogen bonding and salt bridges in proteins was previously shown to decrease the abundance of fragment peaks in other high-energy dissociation methods such as ETD.[46,47] In those instances, additional post-ETD collisional activation was necessary to break the noncovalent interactions between fragments after cleavage of the peptide backbone. It is conceivable that the same effect leads to a decreased abundance of fragments from backbone cleavages around Pro[19] in the *ctt* conformation. This would cause differences in the detection efficiency of fragment ions and lead to the observed differences in UVPD spectra.

Which of the three possibilities described above gives rise to the fragmentation differences reported here is not completely unambiguous although the evidence is most consistent with the third possibility; that is, for ubiquitin 11^+ *cis/trans* isomerization of the peptide bond preceding Pro[19] is very likely the origin for the differences in UVPD fragmentation behavior. What is unambiguous, however, is that the ubiquitin structure and UVPD fragmentation pattern are closely linked. Other possible issues, like the detailed location of charges, await further investigation.
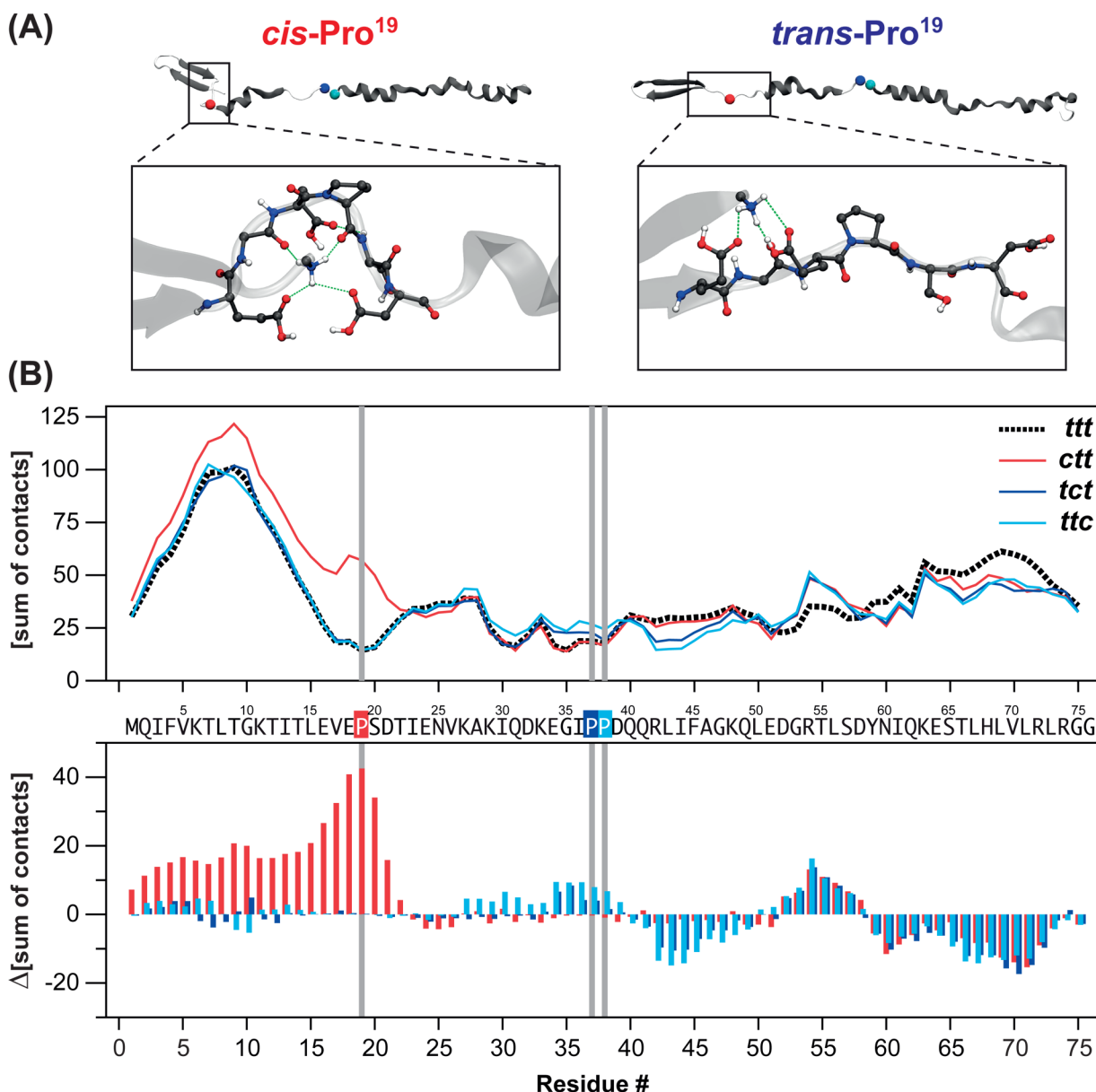
Figure 5. (A) Representative MD snapshots of 11$^+$ ubiquitin and (B) number of intramolecular contacts below 0.3 nm. (A) (left) MD structure with Pro^{19} in *cis* and all other prolines in *trans* conformation (*ctt*); (right) MD structure with all prolines in *trans* conformation (*ttt*). In both structures, the region around Pro^{19} is magnified. (B) (upper panel) number of contacts (atoms being closer than 0.3 nm) between the right and left part of the molecule after a hypothetical cleavage of a peptide bond, where the *x*-axis corresponds to the cleavage position; (lower panel) difference relative to the *ttt* structure. The *ctt* (red) structure shows a considerably elevated number of contacts between the N- and C-terminal fragments when cleaved around Pro^{19}.

CONCLUSIONS

In summary, we provide here the first experimental evidence for the conformational dependency of UV photofragmentation of a protein at 193 nm. In conjunction with MD simulations, results obtained from a combined IMS-MS/UVPD experiment indicate that the *cis/trans* isomerization of proline is responsible for stable A-state-like gas-phase conformations of ubiquitin in high charge states. The *cis/trans* isomerization of the peptide bond preceding Pro^{19} was shown to have the biggest influence on the protein's overall structure when extended, as in the A-state. Seen from a broader perspective, these data furthermore demonstrate the potential of conformer-selective UVPD to serve as tool for the structural analysis of proteins in the gas phase.

ASSOCIATED CONTENT

Ⓢ Supporting Information

Description of the experimental apparatus and typical experimental conditions, data analysis procedures, table of all assigned photofragment peaks, cleavage propensity plot, and CID data. This material is available free of charge via the Internet at http://pubs.acs.org.

AUTHOR INFORMATION

Corresponding Authors
pagel@fhi-berlin.mpg.de
helden@fhi-berlin.mpg.de

■ REFERENCES

(1) Aebersold, R.; Mann, M. *Nature* **2003**, *422*, 198.

(2) Dettmer, K.; Aronov, P. A.; Hammock, B. D. *Mass Spectrom. Rev.* **2007**, *26*, 51.

(3) Polfer, N. C.; Oomens, J. *Mass Spectrom. Rev.* **2009**, *28*, 468.

(4) Wyttenbach, T.; Bowers, M. In *Modern Mass Spectrometry*; Schalley, C. A., Ed.; Springer: Berlin Heidelberg, 2003; Vol. 225, p 207.

(5) Bohrer, B. C.; Merenbloom, S. I.; Koeniger, S. L.; Hilderbrand, A. E.; Clemmer, D. E. *Annu. Rev. Anal. Chem.* **2008**, *1*, 293.

(6) Uetrecht, C.; Rose, R. J.; van Duijn, E.; Lorenzen, K.; Heck, A. J. R. *Chem. Soc. Rev.* **2010**, *39*, 1633.

(7) Bleiholder, C.; Dupuis, N. F.; Wyttenbach, T.; Bowers, M. T. *Nat. Chem.* **2011**, *3*, 172.

(8) Chapman, H. N.; Fromme, P.; Barty, A.; White, T. A.; Kirian, R. A.; Aquila, A.; Hunter, M. S.; Schulz, J.; DePonte, D. P.; Weierstall, U.; Doak, R. B.; Maia, F. R. N. C.; Martin, A. V.; Schlichting, I.; Lomb, L.; Coppola, N.; Shoeman, R. L.; Epp, S. W.; Hartmann, R.; Rolles, D.; Rudenko, A.; Foucar, L.; Kimmel, N.; Weidenspointner, G.; Holl, P.; Liang, M.; Barthelmess, M.; Caleman, C.; Boutet, S.; Bogan, M. J.; Krzywinski, J.; Bostedt, C.; Bajt, S.; Gumprecht, L.; Rudek, B.; Erk, B.; Schmidt, C.; Homke, A.; Reich, C.; Pietschner, D.; Struder, L.; Hauser, G.; Gorke, H.; Ullrich, J.; Herrmann, S.; Schaller, G.; Schopper, F.; Soltau, H.; Kuhnel, K.-U.; Messerschmidt, M.; Bozek, J. D.; Hau-Riege, S. P.; Frank, M.; Hampton, C. Y.; Sierra, R. G.; Starodub, D.; Williams, G. J.; Hajdu, J.; Timneanu, N.; Seibert, M. M.; Andreasson, J.; Rocker, A.; Jonsson, O.; Svenda, M.; Stern, S.; Nass, K.; Andritschke, R.; Schroter, C.-D.; Krasniqi, F.; Bott, M.; Schmidt, K. E.; Wang, X.; Grotjohann, I.; Holton, J. M.; Barends, T. R. M.; Neutze, R.; Marchesini, S.; Fromme, R.; Schorb, S.; Rupp, D.; Adolph, M.; Gorkhover, T.; Andersson, I.; Hirsemann, H.; Potdevin, G.; Graafsma, H.; Nilsson, B.; Spence, J. C. H. *Nature* **2011**, *470*, 73.

(9) Meyer, T.; Gabelica, V.; Grubmüller, H.; Orozco, M. *Wiley Interdiscip. Rev.: Comput. Mol. Sci.* **2013**, *3*, 408.

(10) Wyttenbach, T.; Pierson, N. A.; Clemmer, D. E.; Bowers, M. T. *Annu. Rev. Phys. Chem.* **2014**, *65*, 175.

(11) Ruotolo, B. T.; Giles, K.; Campuzano, I.; Sandercock, A. M.; Bateman, R. H.; Robinson, C. V. *Science* **2005**, *310*, 1658.

(12) Heck, A. J. R. *Nat. Methods* **2008**, *5*, 927.

(13) Ly, T.; Julian, R. R. *Angew. Chem., Int. Ed.* **2009**, *48*, 7130.

(14) Shaw, J. B.; Li, W.; Holden, D. D.; Zhang, Y.; Griep-Raming, J.; Fellers, R. T.; Early, B. P.; Thomas, P. M.; Kelleher, N. L.; Brodbelt, J. S. *J. Am. Chem. Soc.* **2013**, *135*, 12646.

(15) Reilly, J. P. *Mass Spectrom. Rev.* **2009**, *28*, 425.

(16) Choi, K. M.; Yoon, S. H.; Sun, M.; Oh, J. Y.; Moon, J. H.; Kim, M. S. *J. Am. Soc. Mass Spectrom.* **2006**, *17*, 1643.

(17) Guan, Z.; Kelleher, N. L.; O'Connor, P. B.; Aaserud, D. J.; Little, D. P.; McLafferty, F. W. *Int. J. Mass Spectrom. Ion Processes* **1996**, *157−158*, 357.

(18) Kemper, P. R.; Dupuis, N. F.; Bowers, M. T. *Int. J. Mass Spectrom.* **2009**, *287*, 46.

(19) Hess, B.; Kutzner, C.; van der Spoel, D.; Lindahl, E. *J. Chem. Theory Comput.* **2008**, *4*, 435.

(20) Lindorff-Larsen, K.; Piana, S.; Palmo, K.; Maragakis, P.; Klepeis, J. L.; Dror, R. O.; Shaw, D. E. *Proteins* **2010**, *78*, 1950.

(21) Bussi, G.; Donadio, D.; Parrinello, M. *J. Chem. Phys.* **2007**, *126*, No. 014101.

(22) Freitas, M. A.; Hendrickson, C. L.; Emmett, M. R.; Marshall, A. G. *Int. J. Mass Spectrom.* **1999**, *185−187*, 565.

(23) Skinner, O. S.; McLafferty, F. W.; Breuker, K. *J. Am. Soc. Mass Spectrom.* **2012**, *23*, 1011.

(24) Wyttenbach, T.; Bowers, M. T. *J. Phys. Chem. B* **2011**, *115*, 12266.

(25) Koeniger, S. L.; Merenbloom, S. I.; Clemmer, D. E. *J. Phys. Chem. B* **2006**, *110*, 7017.

(26) Myung, S.; Badman, E. R.; Lee, Y. J.; Clemmer, D. E. *J. Phys. Chem. A* **2002**, *106*, 9976.

(27) Koeniger, S. L.; Merenbloom, S. I.; Sevugarajan, S.; Clemmer, D. E. *J. Am. Chem. Soc.* **2006**, *128*, 11713.

(28) Li, J.; Taraszka, J. A.; Counterman, A. E.; Clemmer, D. E. *Int. J. Mass Spectrom.* **1999**, *185−187*, 37.

(29) Shi, H.; Pierson, N. A.; Valentine, S. J.; Clemmer, D. E. *J. Phys. Chem. B* **2012**, *116*, 3344.

(30) Wilkinson, K. D.; Mayer, A. N. *Arch. Biochem. Biophys.* **1986**, *250*, 390.

(31) Pan, Y.; Briggs, M. S. *Biochemistry* **1992**, *31*, 11405.

(32) Brutscher, B.; Bruschweiler, R.; Ernst, R. R. *Biochemistry* **1997**, *36*, 13043.

(33) Badman, E. R.; Hoaglund-Hyzer, C. S.; Clemmer, D. E. *J. Am. Soc. Mass Spectrom.* **2002**, *13*, 719.

(34) Pierson, N. A.; Chen, L.; Russell, D. H.; Clemmer, D. E. *J. Am. Chem. Soc.* **2013**, *135*, 3186.

(35) Breci, L. A.; Tabb, D. L.; Yates, J. R., 3rd; Wysocki, V. H. *Anal. Chem.* **2003**, *75*, 1963.

(36) Kim, P. *Annu. Rev. Biochem.* **1990**, *59*, 631.

(37) Briggs, M. S.; Roder, H. *Proc. Natl. Acad. Sci. U. S. A.* **1992**, *89*, 2027.

(38) Nall, B. T. *Comments Mol. Cell. Biophys.* **1985**, *3*, 123.

(39) Counterman, A. E.; Clemmer, D. E. *Anal. Chem.* **2002**, *74*, 1946.

(40) Baldauf, C.; Pagel, K.; Warnke, S.; von Helden, G.; Koksch, B.; Blum, V.; Scheffler, M. *Chemistry* **2013**, *19*, 11224.

(41) Cordier, F.; Grzesiek, S. *Biochemistry* **2004**, *43*, 11295.

(42) Segev, E.; Wyttenbach, T.; Bowers, M. T.; Gerber, R. B. *Phys. Chem. Chem. Phys.* **2008**, *10*, 3077.

(43) Kony, D. B.; Hunenberger, P. H.; van Gunsteren, W. F. *Protein Sci.* **2007**, *16*, 1101.

(44) Shvartsburg, A. A.; Jarrold, M. F. *Chem. Phys. Lett.* **1996**, *261*, 86.

(45) Pal, D.; Chakrabarti, P. *J. Mol. Biol.* **1999**, *294*, 271.

(46) Lermyte, F.; Konijnenberg, A.; Williams, J. P.; Brown, J. M.; Valkenborg, D.; Sobott, F. *J. Am. Soc. Mass Spectrom.* **2014**, *25*, 343.

(47) Zhang, Z.; Browne, S. J.; Vachet, R. W. *J. Am. Soc. Mass Spectrom.* **2014**, *25*, 604.